Review article

Shumei Chen, Guixin Li*, Kok Wai Cheah, Thomas Zentgraf and Shuang Zhang*

Controlling the phase of optical nonlinearity with plasmonic metasurfaces

https://doi.org/10.1515/nanoph-2018-0011
Received January 26, 2018; revised April 19, 2018; accepted May 9, 2018

Abstract: Metasurfaces are ultrathin structured surfaces that are capable of manipulating the propagation of light in an arbitrary manner. It has been endowed with various functionalities ranging from imaging to holography. In contrast to linear optical processes, the control of wave propagation and diffraction over nonlinear optical processes such as harmonic generations had been much more limited until recently, when the concept of metasurfaces was extended from linear optics to the nonlinear optical regime for manipulating the generation of harmonic signals in an unprecedented level. The key to this recent development lies in the local control over the phase and/or the amplitude of nonlinear polarizability. This new development has led to an array of interesting optical phenomena and nonlinear optical devices that went beyond what had been achieved with traditional nonlinear optical elements. In this review, we summarize the latest progress in controlling the local phase of nonlinearity with plasmonic metasurfaces, with a focus on nonlinear geometric Berry phase and wavefront engineering, and various device applications with nonlinear metasurfaces.

Keywords: nonlinear optics; metasurface; harmonic generation.

***Corresponding authors: Guixin Li,** Department of Materials Science and Engineering, Shenzhen Institute for Quantum Science and Engineering, Southern University of Science and Technology, Shenzhen 518055, China, e-mail: ligx@sustc.edu.cn; and
Shuang Zhang, School of Physics and Astronomy, University of Birmingham, Birmingham, B15 2TT, UK, e-mail: s.zhang@bham.ac.uk
Shumei Chen: School of Physics and Astronomy, University of Birmingham, Birmingham, B15 2TT, UK
Kok Wai Cheah: Department of Physics, Hong Kong Baptist University, Hong Kong, S. A. R. China
Thomas Zentgraf: Department of Physics, University of Paderborn, Warburger Straße 100, D-33098 Paderborn, Germany

1 Introduction

Metamaterials are artificial photonic structures that enable unconventional control of light propagation [1–3]. Electromagnetic properties of the metamaterials can be engineered through the designs of each individual meta-atom. In the last two decades, various exotic optical phenomena such as negative refraction, super-imaging, invisibility, gigantic chirality, and nontrivial topologies have been enabled by metamaterials [1–4]. In particular, the two-dimensional (2D) counterpart of metamaterials, so-called metasurfaces, have attracted growing attention due to their capability of precise control over the wave front of light with relatively easy fabrication procedures [5–8].

A metasurface consists of only a single layer of meta-atoms, which can surprisingly control the wave front very precisely despite its deep subwavelength thickness [5–8]. Over the last few years, many different metasurface designs have been proposed for introducing spatially variant abrupt phase changes across the interface [9–33]. Plasmonic nano-antennas are the most commonly used building blocks, which can strongly interact with light with their ultrathin subwavelength thicknesses. The phase of the transmitted or reflected light depends on both the geometry and orientation of the antennas. In the pioneering work by Yu et al. V-shaped antennas were employed to control the phase of cross-polarized scattered light for a linearly polarized incident beam [5]. The phase manipulation without significant variation in amplitude was enabled by carefully controlled resonances along the two orthogonal directions. Since then, various types of metasurfaces have been realized based on different operating mechanisms. Many interesting optical phenomena have been investigated using metasurfaces, such as extraordinary reflection and transmission, imaging by flat lenses, optical holography, optical spin Hall-Effect, and the generation of optical vortex beams [9–40]. Over the years, the efficiency of the metasurface has been dramatically improved by employing reflective designs or by introducing dielectric resonators [17, 18, 20, 22, 26, 41, 42].

Among the various types of metasurfaces, the so-called geometric phase metasurfaces have gained much popularity due to the simplicity of the phase control by rotating the orientation angle of the constituent meta-atoms of the metasurface [11, 17, 21–24, 29–31]. The precise control over the phase using metasurfaces paves the way towards many practical applications. The underlying mechanisms of the phase control is spin-orbit coupling of light enabled by meta-atoms with anisotropic optical responses [11, 15, 21, 43], which converts the circular polarization state of part of the incident light into its opposite polarization state. The inversion of the circular polarization is accompanied by a geometric phase, or Pancharatnam-Berry (P-B) phase, leading to an antenna orientation controlled phase which does not depend on the specific antenna design or wavelength of light [44–46]. This interesting feature makes its performance broadband and highly robust against fabrication uncertainties.

The concept of metasurfaces has been recently extended to nonlinear optics for manipulating the generation and propagation of nonlinear optical waves [47, 48]. In the past, there has been a large body of works dedicated to the second [49–74] and third harmonic generations (SHG and THG) [75–87] and four-wave-mixing [88–95] in plasmonic metasurfaces. Some of the works have focused on the enhancement of nonlinear conversion due to the plasmonic resonances, while some other works have paid particular attention to the effect of symmetry breaking on SHG. Some of these works were nicely summarized in review articles [96–99]. In this review, we will narrow our scope down to the recent progress of nonlinear photonic metasurfaces for controlling the local nonlinearity phase for harmonic generations. First, we will introduce the concept of nonlinear selection rule for circular polarized fundamental beams. Then, a new approach for precisely controlling the nonlinear optical phase is explained and followed by a discussion of its application in nonlinear holography, imaging, and generation of vortex beams in nonlinear optical processes. Finally, we will briefly summarize and present the outlook of potential future developments of nonlinear metasurfaces.

2 Selection rule for harmonic generations

The symmetry of crystalline structure plays a very important role for harmonic generation processes in a crystal. For example, a necessary condition for even orders of harmonic generation is breaking of inversion symmetry [47, 48]. This also applies to the symmetry of artificial lattice with an engineered crystal structure, such as a plasmonic lattice [49, 50, 56–59, 66, 79, 98]. Recent research has shown that the macroscopic symmetry of metasurfaces also leads to specific selection rules of nonlinear process in a similar way as their microscopic counterpart [100, 101]. As shown in Figure 1A–C, there have been extensive investigations on SHG in plasmonic metasurfaces consisting of building blocks with broken inversion symmetry, such as split ring resonators (SRRs) [49, 57, 65, 66] and L-shaped meta-atoms [50, 56]. Despite the tremendous interest in SHG in plasmonic metasurfaces, not much attention has been paid to the symmetry-governed harmonic processes for a circularly polarized fundamental wave (FW). The circular polarization state representing the spin of photons plays an important role in optics, in particular in the emerging field of spin-orbit coupling of light. A few decades ago, it was discovered that harmonic generation for circularly polarized FWs obeys a selection rule that relates the order of the harmonic process, the rotational symmetry of the crystals, and the circular polarization states of the generated harmonic signals [100, 101]. Recently it was found that the same selection rule can also be applied to plasmonic metasurfaces. This selection rule can be rigorously derived through a simple coordinate transformation process, which is detailed below.

Because of their ultrathin thicknesses, plasmonic meta-atoms that constitute the metasurfaces can be treated as a monolayer array of nonlinear dipole moments. Here we suppose the metasurface is in the X-Y plane. For an incident fundamental light of circular polarization σ along +z direction onto the metasurface, its electric field is expressed as $\vec{E}^{\sigma} = \tilde{E}_0 \hat{e}_{\sigma} = \tilde{E}_0 (\hat{e}_x + i\sigma \hat{e}_y)/\sqrt{2}$, where $\sigma = \pm 1$ represents left- or right-circular polarizations (LCP or RCP). Each plasmonic meta-atom represents a local nonlinear dipole moment. As discussed in Ref. [81], for the mth harmonic generation process, the nonlinear polarization of the plasmonic element can be expressed as

$$\vec{p}^{m\omega} \equiv \vec{p}^{m\omega,\sigma} + \vec{p}^{m\omega,-\sigma} = \ddot{\alpha}_m (\vec{E}^{\sigma})^m \tag{1}$$

where $\ddot{\alpha}_m$ is the mth harmonic nonlinear polarizability tensor of the plasmonic structure. For an ultrathin plasmonic structure under illumination of fundamental beam at normal incidence, the excited nonlinear dipole moment is an in-plane vector, which can be always decomposed into two in-plane counterrotating dipole moments: $\vec{p}^{m\omega,\sigma}$ that has the same rotation direction as the incident circular polarization and $\vec{p}^{m\omega,-\sigma}$ that is opposite to that of the incident fundamental beam. Under a coordinate rotation of $2\pi/n$, where n is the order of rotational symmetry of the structure, both the incident light and the nonlinear dipole

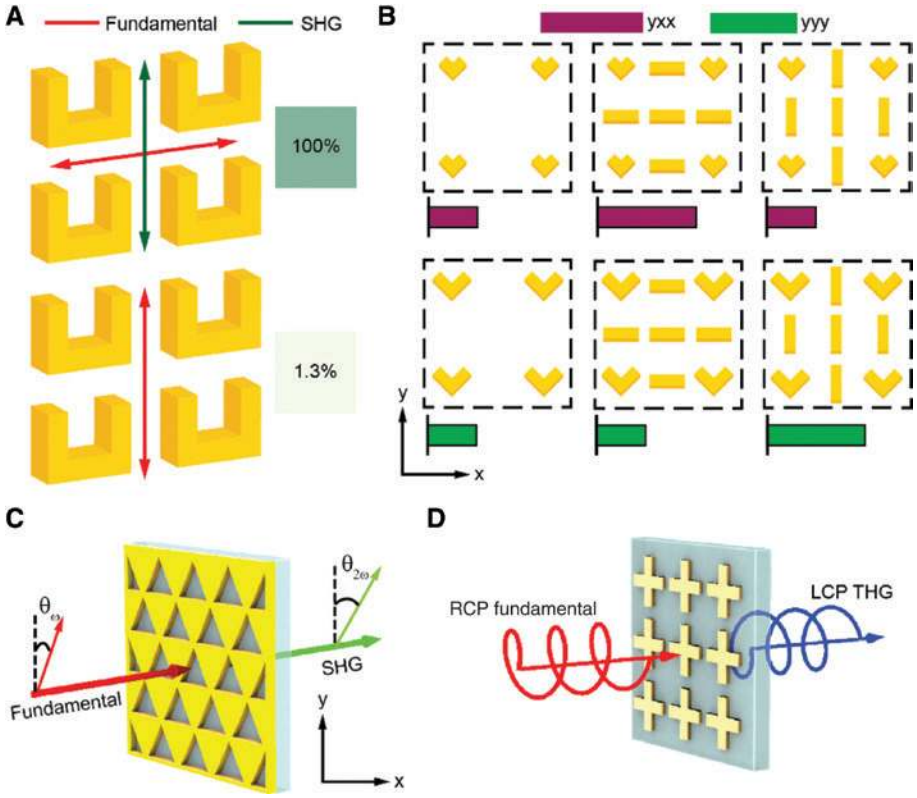

Figure 1: Symmetry consideration in nonlinear plasmonic metasurfaces.
(A) SHG from gold SRRs; (B) SHG from V-shaped plasmonic metasurface; (C) for plasmonic meta-atom with C3 rotational symmetry, the polarization direction of SHG wave exhibits the effect of nonlinear optical activity; (D) for plasmonic meta-atom with C4 rotational symmetry, helicity of THG is opposite to that of FW. A is adapted from Ref. [49], B from Ref. [58], C from Ref. [59], and D from Ref. [79].

moments acquire a spin-dependent phase due to the rotation spin coupling,

$$\vec{E}_T^{\sigma} = \vec{E}^{\sigma} e^{i2\pi\sigma/n}, \vec{p}_T^{m\omega,\sigma} = \vec{p}^{m\omega,\sigma} e^{i2\pi\sigma/n}, \vec{p}_T^{m\omega,-\sigma} = \vec{p}^{m\omega,-\sigma} e^{-i2\pi\sigma/n} \quad (2)$$

where $\vec{E}_T^{\sigma}$, $\vec{p}_T^{m\omega,\sigma}$, and $\vec{p}_T^{m\omega,-\sigma}$ are the electric field of the incident FW and the two nonlinear circular dipole moments in the new coordinate, respectively. Despite the coordinate rotation, the nonlinear polarizability α_m should remain the same because of the n-fold rotational symmetry of the structure. Hence, the nonlinear dipole moments are given by

$$\vec{p}_T^{m\omega,\sigma} + \vec{p}_T^{m\omega,-\sigma} = \vec{\alpha}_m (\vec{E}_T^{\sigma})^m \quad (3)$$

By substituting Eq. (2) into Eq. (3), we have

$$\vec{p}^{m\omega,\sigma} e^{i2\pi\sigma/n} + \vec{p}^{m\omega,-\sigma} e^{-i2\pi\sigma/n} = \vec{\alpha}_m (\vec{E}^{\sigma})^m e^{i2m\pi\sigma/n} \quad (4)$$

By comparing Eq. (4) with Eq. (1), we can readily obtain the following selection rule for the nonlinear harmonic generation:

$$\begin{aligned} \vec{p}^{m\omega,\sigma} &= 0 \quad \text{if } (m-1)/n \text{ is not an integer} \\ \vec{p}^{m\omega,-\sigma} &= 0 \quad \text{if } (m+1)/n \text{ is not an integer} \end{aligned} \quad (5)$$

Equation (5) states that the allowed orders of nonlinear harmonic generation are given by $m=(nl+1)$ for the same circular polarization as the incident wave, and $m=(nl-1)$ for the opposite circular polarization, where l is an arbitrary integer number. Note that in a bulk crystal, the selection rule cannot be applied to the C1 and C2 rotational symmetry because the FW cannot be maintained to be circularly polarized during its propagation inside the crystal. However, this is not an issue for a 2D plasmonic metasurfaces due to the deep subwavelength interaction length.

The above selection rules in the SHG and THG have been independently observed in plasmonic metasurfaces by two groups. In Ref. [59], the SHG from a thin gold film with a hexagonal lattice of circular apertures was investigated. The lattice had a C3 rotational symmetry, i.e. $n=3$. Based on the selection rule, for a circularly polarized incident beam at normal incidence, the allowed orders of harmonic generation with the same circular polarization as the incident beam, given by $m=(nl+1)$, are 1, 4, 7…,

while that with the opposite circular polarization, given by $m=(nl-1)$, are 2, 5, 8…. Hence, for SHG ($m=2$), only nonlinear signal with the opposite circular polarization can be generated. This was confirmed by the experimental result shown in Figure 1C. In a separate work Chen et al. [79] constructed a metasurface consisting of a square lattice array of gold nano-crosses (Figure 1D), in which both the individual building blocks and the lattice exhibit C4 rotational symmetry. Polarization-resolved THG for a circularly polarized FW was measured, which showed that only THG wave of opposite circular polarization as that of the incident wave could be observed. This observation was nicely explained by the nonlinear selection rules [59, 79, 100–103].

3 Controlling the local phase of harmonic generations

Controlling the local phase of nonlinear polarizability plays a very important role in nonlinear optics as it can help compensate the phase mismatch between the fundamental and harmonic generation signals in a nonlinear crystal. This can dramatically enhance the nonlinear conversion efficiency in a bulk crystal [47, 48]. The most commonly employed method for spatially engineering the phase of the nonlinearity (particularly for SHG) is called electric poling [104–106], which involves the application of a strong static electric field to a ferroelectric crystal via patterned electrodes on the crystal surface. For a field strength above the so-called coercive field strength, domain reversal can occur, leading to a change of sign of the second order polarizability. Poling has been mainly applied periodically along a single direction for achieving the so-called quasi-phase matching condition.

Although electric poling has already been successfully employed in practical applications, it has certain limitations. Firstly, electric poling only produces binary phase states (0 and π) for the nonlinear polarizability, which may lead to undesired nonlinear optical processes. In addition, the domain size of the poled ferroelectric materials is usually much larger than the wavelength of light, which can result in multiple diffraction orders in the harmonic signal. Recently, the development of nonlinear metasurfaces provides a new platform to overcome these limitations through a continuous control over the local nonlinear polarizability down to the subwavelength scale [81].

The concept of poling for achieving a binary phase in the nonlinear material polarization has been recently

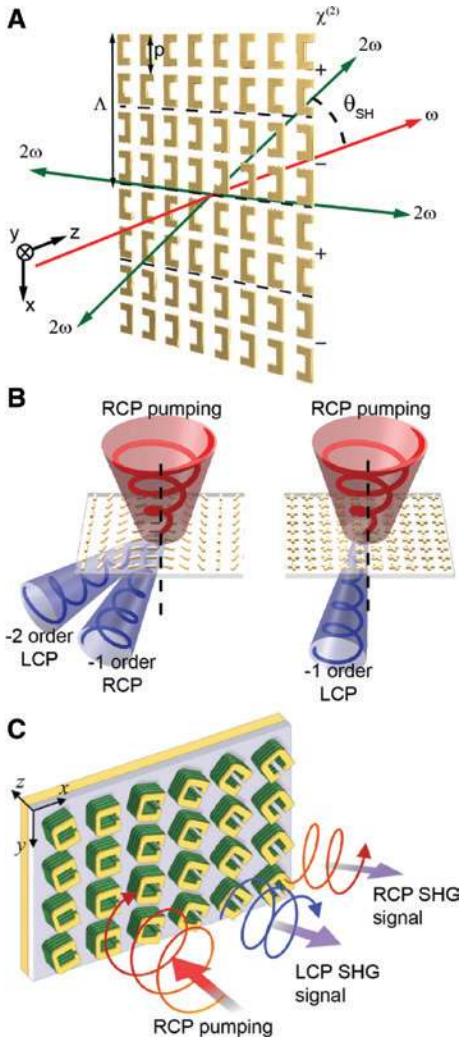

Figure 2: Phase control on nonlinear metasurfaces. (A) Nonlinear metasurface consisting of SRR meta-atoms. The arrangement of the meta-atoms in supercells with opposite orientations introduces π shift of nonlinearity phase for SHG. (B) THG from a nonlinear metasurface based on geometric P-B phase meta-atoms with C2 and C4 symmetry. The continuous phase gradient for the THG signal results in a nonlinear beam deflection. (C) Metal-quantum well hybrid metasurface consists of SRR meta-atoms exhibiting a P-B phase for SHG. A is adapted from Ref. [66], B from Ref. [81], and C from Ref. [70].

applied to the design of nonlinear metasurfaces using "SRR" as the building blocks with sub-wavelength pixel size [66]. There, the mirror symmetry of the SRR was used to reverse the sign of the effective nonlinear susceptibility $\chi^{(2)}$. By simply flipping the orientation of the SRR, a π phase shift of the local SHG radiations can be induced (shown in Figure 2A). Using this concept, Segal et al. demonstrated SHG with well-controlled diffraction angle and achieved a focusing effect for SHG signals. However, for more complex beam manipulation in a nonlinear process

a continuous and spatially variant phase manipulation is more desirable.

Very recently, the concept of the linear P-B phase has been extended to nonlinear harmonic generations of arbitrary orders, paving the way towards the design of nonlinear metasurfaces with continuously controllable phase of the local effective nonlinear polarizability [81]. As shown in Figure 2B and C, the metasurface consists of an array of plasmonic meta-atoms of the same shape but spatially variant orientations. Similar to the proof of nonlinear selection rule, the nonlinear P-B phases can be derived by a coordinate transformation process. For a circularly polarized FW propagating along the rotational axis of a meta-atom, the local effective nonlinear dipole moment can be expressed as $\vec{p}_{\theta}^{n\omega} = \vec{\alpha}_{\theta}(\vec{E}^{\sigma})^n$, where α_{θ} is the nth harmonic nonlinear polarizability tensor of the meta-atom with orientation angle θ, and $\vec{E}^{\sigma}$ is the electric field of FW, with $\sigma=\pm1$ representing the LCP or RCP, respectively. Since the only parameter that distinguishes different meta-atoms is their orientation angle θ, it is natural to assume that α_{θ} is a function of θ. To simplify the derivation, we define a local coordinate (referred to as local frame) which is attached to each meta-atom. Hence, the local coordinate (x', y') axes are rotated by an angle of θ with respect to the laboratory frame (x, y). Similar to Eq. (2), the incident light acquires a spin-dependent phase due to the rotation spin coupling [81],

$$\vec{E}_L^{\sigma} = \vec{E}^{\sigma} \mathrm{e}^{i\sigma\theta} \tag{6}$$

where the index "L" denotes the meta-atom's local coordinate frame. Since the local coordinate is fixed, the nth harmonic nonlinear polarizability of the meta-atom's local frame is simply $\alpha(0)$. Thus, the nth harmonic nonlinear dipole moment in the local frame is given by

$$\vec{p}_{\theta,L}^{n\omega} = \vec{\alpha}_0(\vec{E}_L^{\sigma})^n = \vec{\alpha}_0(\vec{E}^{\sigma})^n e^{in\sigma\theta} \tag{7}$$

Due to the ultrathin thickness of the meta-atoms, it is safe to assume that the nonlinear dipole moment lies in the X-Y plane, which can be further decomposed into two in-plane counter-rotating dipole moments as

$$\vec{p}_{\theta,L}^{n\omega} = \vec{p}_{\theta,L,\sigma}^{n\omega} + \vec{p}_{\theta,\mathrm{L},-\sigma}^{n\omega} \tag{8}$$

We finally make a transformation from the local frame back to the laboratory frame, with the two rotating dipole moments expressed as

$$\begin{aligned} \vec{p}_{\theta,\sigma}^{n\omega} &= \vec{p}_{\theta,L,\sigma}^{n\omega} e^{-i\sigma\theta} \propto e^{(n-1)i\sigma\theta} \\ \vec{p}_{\theta,-\sigma}^{n\omega} &= \vec{p}_{\theta,L,-\sigma}^{n\omega} e^{i\sigma\theta} \propto e^{(n+1)i\sigma\theta} \end{aligned} \tag{9}$$

Hence, the nonlinear polarizabilities of the individual meta-atom are given by

$$\begin{aligned} \alpha_{\theta,\sigma,\sigma}^{n\omega} &\propto e^{(n-1)i\sigma\theta} \\ \alpha_{\theta,-\sigma,\sigma}^{n\omega} &\propto e^{(n+1)i\sigma\theta} \end{aligned} \tag{10}$$

Equation (10) shows that the nth nonlinear polarizability of a meta-atom contains two circular components with different angle-dependent phases; the one with the same circular polarization as the FW has a phase of $(n-1)\sigma\theta$, and the other with the opposite circular polarization has a phase of $(n+1)\sigma\theta$. However, based on the rotational symmetry of the meta-atom, one or both of the circular components of the nonlinear polarizability may not be present, according to the aforementioned nonlinear selection rules [59, 81, 100–103].

The continuous phase control over the nonlinearity was recently experimentally demonstrated. In Ref. [81], phase control over THG wave was demonstrated by using metasurfaces consisting of plasmonic meta-atoms with two- and four-fold rotational symmetries (Figure 2B). For a meta-atom with two-fold rotational symmetry (C2), THG signals with both the same and opposite circular polarizations as the FW can be generated with a spin-dependent phase of $2\sigma\theta$ and $4\sigma\theta$, respectively (Figure 3A). On the other hand, a meta-atom with three- and four-fold rotational symmetry (C4) prohibits the generation of the SHG and THG signal with the same polarization state as the incident polarization. Hence, only a single SHG and THG signal with opposite circular polarizations to that of the incident FW is generated with a geometric phase of $3\sigma\theta$ and $4\sigma\theta$, respectively (Figure 3B and C).

To precisely measure the third-order nonlinearity phase, a nonlinear phase meta-grating was designed, which consisted of supercells composed of two sets of antennas of different orientation angles. As the periodicity of the supercell was greater than the third harmonic wavelength, for an incident FW, there existed at least the first diffraction orders for the THG signal. The relative intensities of the 0th and the 1st orders are determined by the nonlinearity phase difference between the two sets of antennas making up the supercell. For the two sets of gratings forming an angle of 45°, the corresponding nonlinearity phase between them was 180°, which resulted in a completely destructive interference in the 0th order.

Thus, by exploiting the rotational symmetry of the meta-atoms (such as C4 symmetry for THG and C3 symmetry for SHG), only a single circularly polarized

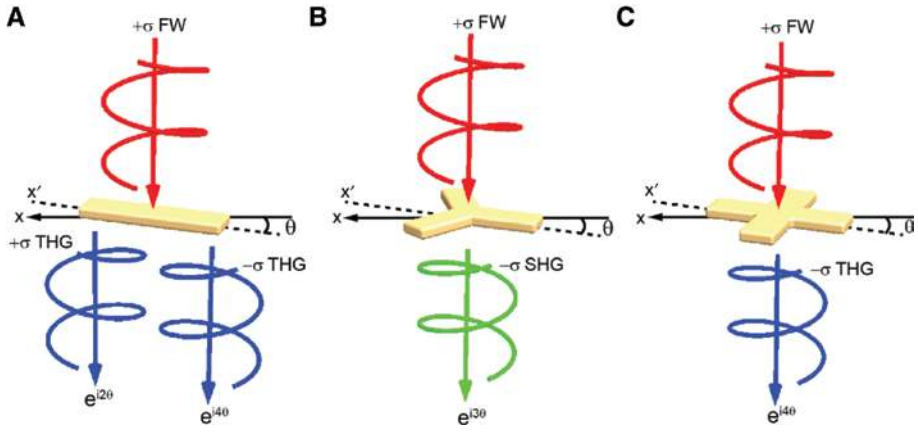

Figure 3: Nonlinear geometric P-B phase elements.
(A–C) Nonlinear phase elements with two-, three-, and four-fold rotational symmetry (C2–C4). Based on the rotational symmetry, only particular nonlinear processes and circular polarization states are allowed. (A) SHG from a C2 symmetric structure is forbidden; the P-B phases of 2θ and 4θ for the THG are observed. (B) For a C3 meta-atom, the P-B phase of SHG with opposite helicity compared to the FW is 3θ. (C) SHG from C4 meta-atoms is forbidden, and the P-B phase for the THG with opposite circular polarization is equal to 4θ. θ is the orientation angle of the meta-atom. A–C are adapted from Ref. [98].

harmonic generation signal exists with well-defined nonlinearity phase. Importantly, for rotational symmetry order greater than two, each meta-atom has isotropic electromagnetic responses in the in-plane directions, which is very similar to a circular disk. In this case, the linear optical response of each antenna does not depend on its orientation, and therefore the linear optical response is decoupled from its nonlinear optical responses. For example, by assembling meta-atoms of C3 or C4 rotational symmetries with spatially varying orientations in a 2D lattice or 3D lattice, a nonlinear metasurface or metamaterial can be formed which shows homogeneous linear properties but locally an inhomogeneous nonlinear polarizability distribution for a circularly polarized FW.

While a single harmonic signal with well-defined phase is usually preferred, multiple nonlinear signals with different phases can sometimes be useful for information multiplexing in holography. In such cases, meta-atoms with the lowest rotational symmetry, i.e. C1 symmetry, such as SRRs, can be used. For example, SRRs can generate a phase shift of $\sigma\theta$ and $3\sigma\theta$ for SHG signals of different circular polarizations [70, 71] (Figure 2C). In Figure 3, by taking into account the nonlinear selection rules, we summarize the angle-dependent nonlinearity phase for different orders of harmonic generation and for nanoantennas of various rotational symmetries. The nonlinear Berry phase provides a powerful yet simple route to controlling the wavefront of nonlinear optical radiation without affecting the uniformity of the linear optical response.

4 Device applications of nonlinear metasurfaces

4.1 Nonlinear metasurface holography

In the linear optical regime, due to their superior capability of phase manipulation, metasurfaces have been used for various practical applications, such as flat lenses [11, 26] and optical holography [13, 14, 19–24, 31, 107]. Extending the techniques of linear optical wavefront engineering to the nonlinear optical regime leads to a demonstration of various optical functionalities, such as nonlinear holography, nonlinear imaging, and nonlinear spin-orbit interaction of light. Combining the concept of multiplexed phase control for nonlinear signals of different polarization states with holography optimization techniques, multiple holographic images (Figure 4A and B) can be generated that are multiplexed by the polarization state of the FW, the nonlinear signals, or both [71, 86].

Recently, it was shown that a nonlinear metasurface consisting of an array of SRRs with spatially variant orientations could be used to generate three completely independent holographic images in the transmitted waves of the fundamental and the second harmonic wavelengths [71]. For a circularly polarized FW with a spin σ incident onto a SRR metasurface with an orientation angle of φ, the transmitted beam with spin $-\sigma$ at the fundamental wavelength acquires a geometric P-B phase of $2\sigma\varphi$. Meanwhile, the SHG signals of both spins can be generated due to the C1 rotational symmetry of the SRR. Both the SHG signals

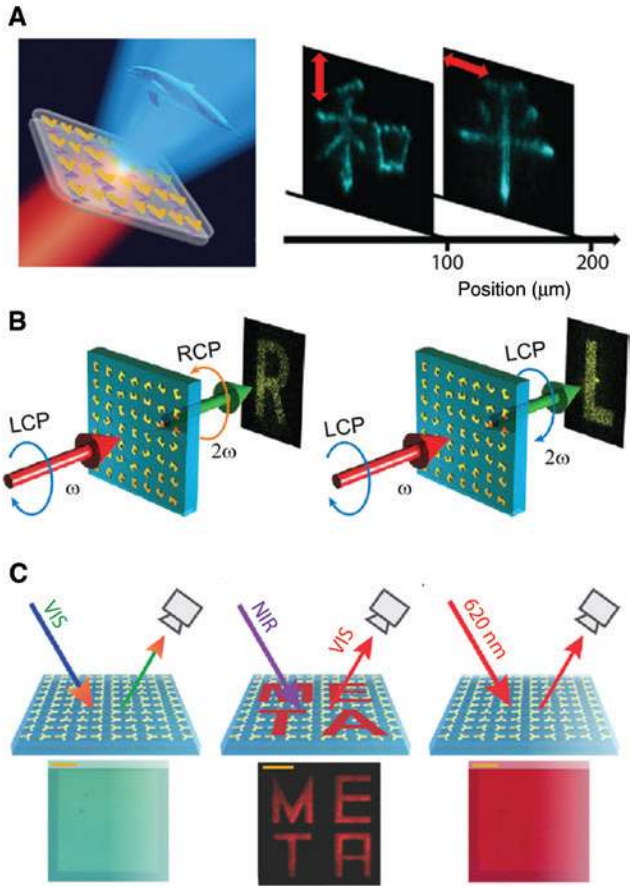

Figure 4: Nonlinear optical holography and encryption. (A) Nonlinear metasurface holography. The local P-B phase of SHG wave comes from the orientation of the SRR meta-atoms and circular polarization of FW. This technique allows encoding different images into one metasurface using two opposite polarization states, which correspond to different P-B phases. (B) Nonlinear holography using THG from V-shaped meta-atoms. (C) Nonlinear metasurface for information encryption. If the metasurface is illuminated with unpolarized white light, no image can be observed. Under pumping of circularly polarized FW at the wavelength of 1240 nm, an image with the characters "META" appears at the SHG wavelength (620 nm); for a direct illumination with unpolarized light at a wavelength of 620 nm, no information on the "META" characters is observed. A is adapted from Ref. [86], B from Ref. [71], and C from Ref. [73].

with spin σ and $-\sigma$ can be generated, which acquire a nonlinear Berry phase of $\sigma\varphi$ and $3\sigma\varphi$, respectively [71]. In this case, the linear and nonlinear geometric phases, corresponding to optical signals of different frequencies and different spins, are correlated to each other. Nevertheless, three independent holographic images can be designed by utilizing a single metasurface, which was designed using an improved Fidoc algorithm. Experimentally, three independent holographic images of the letters "R" and "L" were observed with frequency/spin combinations of $(2\omega, -\sigma)$ and $(2\omega, \sigma)$, respectively (Figure 4A). In another work, Almeida et al. [86] constructed a double-layer nonlinear metasurface holography, with each layer operating for FW with one particular linear polarization only. The cross talk between the two layers was minimized due to the orthogonality between the polarization states of light that the two layers could interact with. Experimentally, two independent images were observed at the SHG wavelength, which were multiplexed by using the linear polarization states of the FW. The polarization and/or wavelength-dependent nonlinear metasurface holography presented above may have applications in multi-dimensional optical data storages and optical encryptions.

4.2 Nonlinear metasurface encryption

Not only the phase but also the magnitude of the nonlinear signals can be controlled by designing a supercell that consists of multiple meta-atoms of different orientations. Recently, it was shown that nonlinear metasurfaces could be used to encode grey scale images in the SHG, while no images appear at fundamental wavelength [108]. This feature is very useful for information encryption. The nonlinear metasurface consists of an array of C3 plasmonic meta-atoms. Each supercell of the metasurface comprises two meta-atoms of different orientations. The intensity of the SHG signal generated by each supercell could be continuously tuned by controlling the relative orientation angle between the two meta-atoms within a supercell. The maximum SHG intensity was achieved when the two meta-atoms have the same orientations, while a minimum intensity of 0 could arise from a complete destructive interference of SHG waves when the relative orientation angle between them is 60°. In one of the metasurface designs, an image of the word "META" was encoded. The supercells of the background and the letters consisted of C3 meta-atoms with relative orientation angle of $\theta = 60°$ and $\theta = 0°$, respectively, leading to the destructive and constructive interferences, respectively (Figure 4C). In this way, an image of the encoded letters "META" becomes visible at the SHG wavelength. However, the "META" letters are hidden in the metasurface if only the linear optical measurement was applied, as shown by Figure 4C, where only a nearly homogenous background signal was observed.

4.3 Nonlinear metasurface lens

The first nonlinear metasurface lens in the form of a Fresnel zone plate was demonstrated by Segal et al. [66].

The nonlinear zone plate consisted of annular zones, with adjacent zones composed of SRRs of opposite directions, leading to binary nonlinear phases of 0 and π. This was a direct analogue of poling along an in-plane direction. For an incident Gaussian FW, focused SHG signal in the transmission direction was observed. A focal spot of 7 μm with an enhancement of 73-fold in intensity relative to the SHG at the metasurface was observed. Nonlinear metasurface lens was also demonstrated for four-wave mixing (FWM) by Almeida et al. [94]. The metasurface consisted of an array of rectangular apertures in a gold film. The phase of the nonlinear signal generated by each aperture was controlled by its width and length. Based on this, a series of nonlinear metasurfaces were designed and fabricated, which focused the FWM signal at different focal distances ranging from 5 to 30 μm.

In the above demonstrations, the quality of focusing was limited by either the binary phase or inaccurate control over the nonlinearity phase. Very recently, nonlinear P-B phase was employed for the design of high quality nonlinear metasurface lenses that were capable of focusing generated SHG signal into a diffraction-limited spot. As shown by the scanning electron microsopy image in Figure 5A, the nonlinear metalens consisted of an array of meta-atoms of C3 rotational symmetry, with the orientation angle of each meta-atom satisfying

$$\theta(\mathrm{r}) = k_0(\sqrt{f^2 + \mathrm{r}^2} - |f|)/3 \tag{11}$$

where r is the distance from the axis of the metalens, f is the focal length of the lens, and $k_0 = \frac{2\pi}{\lambda}$ is the free-space wave vector of the SHG wave. The nonlinear metalens had a diameter of 300 μm, and the C3 nano-antennas were positioned on concentric rings with a spacing of 500 nm. For a metalens designed at $f = 500$ μm, the measured SHG intensity distribution at different transverse planes in the focal region is shown in Figure 5A, where a diffraction-limited spot is observed. In the experiment, an L-shaped aperture carved into a metal film served as the object, which was positioned at a certain distance in front of the nonlinear metalens. A circularly polarized FW was used to illuminate the "L" aperture. The transmitted wave interacted with the nonlinear metalens, where the SHG waves were generated and imaged in the transmission direction due to the nonlinearity phase distribution across the metalens (Figure 5A). More interestingly, due to the spin-dependent nature of the nonlinear P-B phase, the nonlinear metalens could function either as a convex lens or a concave lens, resulting in formation of real or virtual images depending on the circular polarization states of the FW.

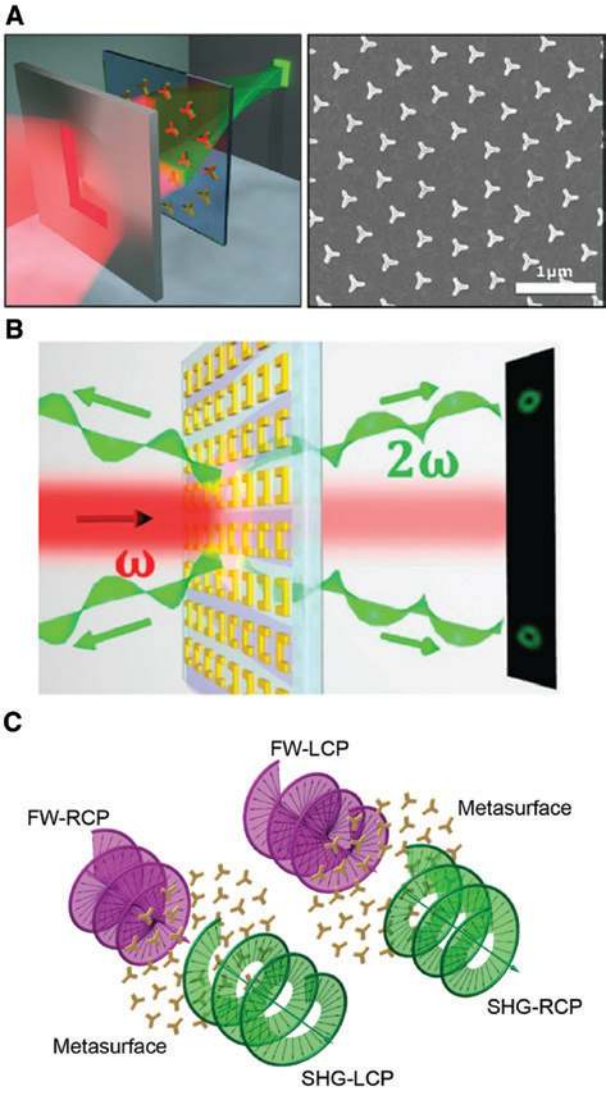

Figure 5: Metasurface for nonlinear imaging and wavefront engineering.
(A) Working principle of the nonlinear metalens. Illustration of the imaging concept: An L-shaped aperture is imaged on a screen with the help of the nonlinear metalens consisting of C3 nanoantennas (right). (B) SHG beam with OAM was generated using SRR metasurface with fork-type singularity. (C) Schematic of spin controlled generation of OAM of SHG by using nonlinear photonic metasurface. For an FW with two spin states (LCP and RCP) normally incident onto the nonlinear photonic metasurface with C3 symmetry, generation of SHG waves with opposite handiness to that of FW is allowed. By encoding the phase singularity into the metasurfaces, the SHG vortex beams with spin controlled topological charges are obtained. A is adapted from Ref. [108], B from Ref. [72], and C from Ref. [73, 74].

4.4 Nonlinear vortex beam generation

Optical vortex beams possessing orbit angular momentum (OAM) [109] are promising for classical and quantum optical communications [110–112]. In the past few years,

generation of vortex beams using metasurfaces in the linear optical regime has been widely explored [15, 28, 29]. Precise control over the local nonlinearity phase in metasurfaces has provided the opportunity to combine the functionalities of nonlinear harmonic generations and wavefront engineering into a single nonlinear metasurface [81]. There have been two different approaches to realize direct generation of nonlinear vortex beams using metasurfaces, based on fork grating [72, 113] and nonlinear P-B phase [74], respectively.

In the first approach, a gold fork grating with topological charge of q was fabricated. A FW was incident onto the fork grating, which was designed such that the periodicity was greater than the wavelength of the harmonic generation signals. In transmission direction, vortex beams at both the SHG and THG wavelengths were observed in the first diffraction orders. Both the harmonic signals carried the topological charge of the fork grating, i.e. $l = q$.

More powerful control over the nonlinearity phase can be realized by exploiting the nonlinear P-B phase in a metasurface. In a recent work by Li et al. [74], metasurfaces based on nonlinear P-B phase were used to generate vortex beams with spin angular momentum [114] for the SHG wave. The nonlinear metasurfaces consisted of gold meta-atoms with three-fold (C3) rotational symmetry (Figure 5C). Based on the nonlinear selection rules, for a circularly polarized FW, only SHG with opposite circular polarization state to that of the FW is allowed, and the nonlinear P-B phase of each C3 meta-atom is $3\sigma\theta$, where θ is the in-plane orientation angle of the meta-atom. Three plasmonic metasurfaces with different topological charges were demonstrated, and high quality vortex beams were experimentally observed. For linearly polarized FW that comprises both LCP and RCP components, two SHG vortex beams of opposite spins and opposite OAMs were simultaneously generated, which were overlapping with each other. By selecting a linear polarization from the two combined SHG vortices of opposite circular polarizations, the interference pattern of the two OAM modes results in a Hermite-Gaussian mode with a petal number double the OAM number of the vortex beams.

5 Conclusions/perspective

In this review, we presented the recent development of nonlinear metasurfaces for locally controlling the nonlinearity phase of the harmonic generations. We have focused on harmonic generations with circularly incident FW, where the rotational symmetry of the meta-atoms plays a very important role. We first discussed the nonlinear selection rule that dictates the allowable harmonic generation orders for a particular rotational symmetry of the meta-atom. We then extended the concept of P-B phase from linear optics to nonlinear optics, which features a simple relationship between the orientation angle of the meta-atom and the local nonlinearity phase. We discussed a number of applications with nonlinear metasurfaces, such as nonlinear holography, vortex beam generation, and nonlinear metalenses. Nonlinear P-B phase provides us unprecedented level of control over the wavefront of the harmonic waves. However, the conversion efficiency of nonlinear metasurfaces is still very low. Therefore, new nonlinear materials and systems, such as semiconductors with intersubband transition, need to be exploited in the future to enhance the efficiency of nonlinear optical conversions. In addition, by extending the concept of P-B phase from 2D metasurfaces to 3D metamaterials, the local control over the nonlinear optical phase may help design novel optical devices satisfying the phase matching condition for harmonic generations. Then it is possible to develop highly efficient nonlinear photonic devices, which have great potential for applications in optical sensing, imaging, and communications. Moreover, the study of the spin-orbit interaction with nonlinear optical metasurface provides a versatile platform for high-dimensional classical and quantum optical communications. With the further development of the functionalities and efficiencies of nonlinear metasurfaces, we would like to expect an increasing amount of applications and new research fields based on the platform of nonlinear optical metasurface devices.

Acknowledgments: This work was financially supported by the Marie Curie Individual Fellowship (Grant H2020-MSCA-IF-703803-NonlinearMeta) and the European Research Council Consolidator Grant (TOPOLOGICAL). G. L. acknowledges the support from the National Natural Science Foundation of China (11774145), Natural Science Foundation of Shenzhen Innovation Committee (JCYJ20170412153113701), and Applied Science and Technology Project of Guangdong Science and Technology Department (2017B090918001).

References

[1] Soukoulis CM, Wegener M. Past achievements and future challenges in the development of three-dimensional photonic metamaterials. Nat Photon 2011;5:523–30.
[2] Zheludev NI, Kivshar YS. From metamaterials to metadevices. Nat Mater 2012;11:917–24.
[3] Pendry JB, Luo Y, Zhao R. Transforming the optical landscape. Science 2015;348:521–4.

[4] Gao W, Lawrence M, Yang B, et al. Topological photonic phase in chiral hyperbolic metamaterials. Phys Rev Lett 2015;114:037402.
[5] Yu N, Genevet P, Kats MA, et al. Light propagation with phase discontinuities: generalized laws of reflection and refraction. Science 2011;334:333–7.
[6] Kildishev AV, Boltasseva A, Shalaev VM. Planar photonics with metasurfaces. Science 2013;339:1232009.
[7] Meinzer N, Barnes WL, Hooper IR. Plasmonic meta-atoms and metasurfaces. Nat Photon 2014;8:889–98.
[8] Yu N, Capasso F. Flat optics with designer metasurfaces. Nat Mater 2014;13:139–50.
[9] Ni X, Emani NK, Kildishev A, Boltasseva VA, Shalaev VM. Broadband light bending with plasmonic nanoantennas. Science 2012;335:427.
[10] Sun S, He Q, Xiao S, Xu Q, Li X, Zhou L. Gradient-index metasurfaces as a bridge linking propagating waves and surface waves. Nat Mater 2012;11:426–31.
[11] Chen X, Huang L, Mühlenbernd H, et al. Dual-polarity plasmonic metalens for visible light. Nat Commun 2012;3:1198.
[12] Chen WT, Yang KY, Wang CM, et al. High-efficiency broadband meta-hologram with polarization controlled dual images. Nano Lett 2013;14:225–30.
[13] Ni X, Kildishev AV, Shalaev VM. Metasurface holograms for visible light. Nat Commun 2013;4:2807.
[14] Huang L, Chen X, Mühlenbernd H, et al. Three-dimensional optical holography using a plasmonic metasurface. Nat Commun 2013;4:2808.
[15] Li G, Kang M, Chen S, et al. Spin-enabled plasmonic metasurfaces for manipulating orbital angular momentum of light. Nano Lett 2013;13:4148–51.
[16] Yin XB, Ye ZL, Rho J, Wang Y, Zhang X. Photonic spin Hall effect at metasurfaces. Science 2013;339:1405–7.
[17] Lin D, Fan P, Hasman E, Brongersma ML. Dielectric gradient metasurface optical elements. Science 2013;345:298.
[18] Khorasaninejad M, Crozier KB. Silicon nanofin grating as a miniature chirality-distinguishing beam-splitter. Nat Commun 2014;5:5386.
[19] Huang YW, Chen WT, Tsai WY, et al. Aluminum plasmonic multicolor meta-hologram. Nano Lett 2015;15:3122–7.
[20] Chong KE, Staude I, James A, et al. Polarization-independent silicon metadevices for efficient optical wavefront control. Nano Lett 2015;15:5369–74.
[21] Zheng G, Mühlenbernd H, Kenney M, Li G, Thomas Z, Zhang S. Metasurface holograms reaching 80% efficiency. Nat Nanotech 2015;10:308–12.
[22] Arbabi A, Horie Y, Bagheri M, Faraon A. Dielectric metasurfaces for complete control of phase and polarization with subwavelength spatial resolution and high transmission. Nat Nanotech 2015;10:937–43.
[23] Huang L, Mühlenbernd H, Li X, et al. Broadband hybrid holographic multiplexing with geometric metasurfaces. Adv Mater 2015;27:6444–9.
[24] Wen D, Yue F, Li G, et al. Helicity multiplexed broadband metasurface holograms. Nat Commun 2015;6:8241.
[25] Aieta F, Kats MA, Genevet P, Capasso F. Multiwavelength achromatic metasurfaces by dispersive phase compensation. Science 2015;347:1342–5.
[26] Khorasaninejad M, Chen WT, Devlin RC, Oh J, Zhu AY, Capasso F. Metalenses at visible wavelengths: diffraction-limited focusing and subwavelength resolution imaging. Science 2016;352:1190–4.
[27] Wang Q, Rogers E, Gholipour B, et al. Optically reconfigurable metasurfaces and photonic devices based on phase change materials. Nat Photon 2016;10:60–5.
[28] Maguid E, Yulevich I, Veksler D, Kleiner V, Brongersma ML, Hasman E. Photonic spin-controlled multifunctional shared-aperture antenna array. Science 2016;352:1202–6.
[29] Chen S, Cai Y, Li G, Zhang S, Cheah KW. Geometric metasurface fork gratings for vortex beam generation and manipulation. Laser Photon Rev 2016;2:322–6.
[30] Arbabi A, Arbabi E, Horie Y, Kamali SM, Faraon A. Planar metasurface retroreflector. Nat Photon 2017;11:415–20.
[31] Balthasar Mueller JP, Rubin NA, Devlin RC, Groever B, Capasso F. Metasurface polarization optics: independent phase control of arbitrary orthogonal states of polarization. Phys Rev Lett 2017;118:113901.
[32] Avayu O, Almeida E, Prior Y, Ellenbogen T. Composite functional metasurfaces for multispectral achromatic optics. Nat Commun 2017;8:14992.
[33] Wang S, Wu PC, Su VC, et al. Broadband achromatic optical metasurface devices. Nat Commun 2017;8:187.
[34] Maguid E, Yannai M, Faeman A, Yulevich I, Kleiner V, Hasman E. Disorder-induced optical transition from spin Hall to random Rashba effect. Science 2017;358:1411–5.
[35] Devlin RC, Ambrosio A, Rubin NA, Capasso F. Arbitrary spin-to-orbital angular momentum conversion of light. Science 2017;358:896–901.
[36] Khorasaninejad M, Capasso F. Metalenses: versatile multifunctional photonic components. Science 2017; 10.1126/science.aam8100.
[37] Deng Z, Li G. Metasurface optical holography. Mater Today Phys 2017;3:16–32.
[38] Wang S, Wu PC, Su VC, et al. A broadband achromatic metalens in the visible. Nat Nanotech 2018;13:227–32.
[39] Chen WT, Zhu AY, Sanjeev V, et al. A broadband achromatic metalens for focusing and imaging in the visible. Nat Nanotech 2018;13:220–6.
[40] Deng ZL, Deng JH, Zhuang X, et al. Diatomic metasurface for vectorial holography. Nano Lett 2018;18:2885–92.
[41] Pfeiffer M, Kordts A, Brasch V, et al. Photonic Damascene process for integrated high-Q microresonator based nonlinear photonics. Optica 2016;3:20–5.
[42] Xu K, Liu H, Zhang Z. Gate-controlled diode structure based electro-optical interfaces in standard silicon-CMOS integrated circuitry. Appl Opt 2015;54:6420–4.
[43] Bliokh KY, Rodriguez-Fortuno FJ, Nori F, Zayats AV. Spin-orbit interactions of light. Nat Photon 2015;9:796–808.
[44] Pancharatnam S. Generalized theory of interference, and its applications. Part I. Coherent pencils. Proc Indian Acad Sci Sect A 1956;44:247–62.
[45] Berry MV. Quantal phase factors accompanying adiabatic changes. Proc R Soc London Ser A 1984;392:45–57.
[46] Bornzon Z, Biener G, Kleiner V, Hasman E. Space-variant Pancharatnam Berry phase optical elements with computer-generated subwavelength gratings. Opt Lett 2002;27:1141–3.
[47] Shen YR. The principles of nonlinear optics. New York, John Wiley, 1984.
[48] Boyd RW. Nonlinear optics, 3rd ed. New York, Academic Press, 2008.

[49] Klein MW, Enkrich C, Wegener M, Linden S. Second-harmonic generation from magnetic metamaterials. Science 2006;313:502–4.
[50] Kujala S, Canfield BK, Kauranen M, Svirko Y, Turunen J. Multipole interference in the second-harmonic optical radiation from gold nanoparticles. Phys Rev Lett 2007;98:167403.
[51] Valev VK, Silhanek AV, Verellen N, et al. Asymmetric optical second-harmonic generation from chiral G-shaped gold nanostructures. Phys Rev Lett 2010;104:127401.
[52] Zhang Y, Grady NK, Ayala-Orozco C, Halas NJ. Three-dimensional nanostructures as highly efficient generators of second harmonic light. Nano Lett 2011;11:5519–23.
[53] Rose A, Huang D, Smith DR. Controlling the second harmonic in a phase matched negative-index metamaterial. Phys Rev Lett 2011;107:063902.
[54] Cai W, Vasudev AP, Brongersma ML. Electrically controlled nonlinear generation flight with plasmonics. Science 2011;333:1720–3.
[55] Aouani H, Navarro-Cia M, Rahmani M, et al. Multiresonant broadband optical antennas as efficient tunable nanosources of second harmonic light. Nano Lett 2012;12:4997–5002.
[56] Husu H, Siikanen R, Mäkitalo J, et al. Metamaterials with tailored nonlinear optical response. Nano Lett 2012;12:673–7.
[57] Linden S, Niesler F, Forstner J, Grynko Y, Meier T, Wegener M. Collective effects in second-harmonic generation from split-ring-resonator arrays. Phys Rev Lett 2012;109:015502.
[58] Czaplicki R, Husu H, Siikanen R, Makitalo J, Kauranen M. Enhancement of second-harmonic generation from metal nanoparticles by passive elements. Phys Rev Lett 2013;110:093902.
[59] Konishi K, Higuchi T, Li J, Larsson J, Ishii S, Kuwata-Gonokami M. Polarization-controlled circular second-harmonic generation from metal hole arrays with threefold rotational symmetry. Phys Rev Lett 2014;112:135502.
[60] Rodrigues SP, Lan S, Kang L, Cui Y, Cai W. Nonlinear imaging and spectroscopy of chiral metamaterials. Adv Mater 2014;26:6157–62.
[61] Cox JD, Garcia de Abajo FJ. Electrically tunable nonlinear plasmonics in graphene nanoislands. Nat Commun 2014;5:5725.
[62] Lee J, Tymchenko M, Argyropoulos C, et al. Giant nonlinear response from plasmonic metasurfaces coupled to intersubband transitions. Nature 2014;511:65–9.
[63] Lan S, Kang L, Schoen DT, et al. Backward phase-matching for nonlinear optical generation in negative-index materials. Nat Mater 2015;14:807–11.
[64] Seyler KL, Schaibley JR, Gong P, et al. Electrical control of second harmonic generation in a WSe_2 monolayer transistor. Nat Nanotech 2015;10:407–11.
[65] O'Brien K, Suchowski H, Rho J, et al. Predicting nonlinear properties of metamaterials from the linear response. Nat Mater 2015;14:379–83.
[66] Segal N, Keren-Zur S, Hendler N, Ellenbogen T. Controlling light with metamaterial-based nonlinear photonic crystals. Nat Photon 2015;9:180–4.
[67] Celebrano M, Wu X, Baselli M, et al. Mode matching in multiresonant plasmonic nanoantennas for enhanced second harmonic generation. Nat Nanotech 2015;10:412–7.
[68] KrukS, Weismann M, Yu A, et al. Enhanced magnetic second-harmonic generation from resonant metasurfaces. ACS Photon 2015;2:1007–12.
[69] Sartorello G, Olivier N, Zhang J, et al. Ultrafast optical modulation of second- and third-harmonic generation from cut-disk-based metasurfaces. ACS Photon 2016;3:1517–22.
[70] Tymchenko M, Sebastian Gomez-Diaz J, Lee J, et al. Gradient nonlinear Pancharatnam-Berry metasurfaces. Phys Rev Lett 2016;107:207403.
[71] Ye W, Zeuner F, Li X, et al. Spin and wavelength multiplexed nonlinear metasurface holography. Nat Commun 2016;7:11930.
[72] Keren-Zur S, Avayu O, Michaeli L, Ellenbogen T. Nonlinear beam shaping with plasmonic metasurfaces. ACS Photon 2016;3:117–23.
[73] Walter F, Li G, Meier C, Zhang S, Zentgraf T. Ultrathin nonlinear metasurface for optical image encoding. Nano Lett 2017;17:3171–5.
[74] Li G, Wu L, Li KF, et al. Nonlinear metasurface for simultaneous control of spin and orbital angular momentum in second harmonic generation. Nano Lett 2017;17:7974–9.
[75] Utikal T, Zentgraf T, Paul T, et al. Towards the origin of the nonlinear response in hybrid plasmonic systems. Phys Rev Lett 2011;106:133901.
[76] Liu H, Li G, Li KF, et al. Linear and nonlinear Fano resonance on two-dimensional magnetic metamaterials. Phys Rev B 2011;84:235437.
[77] Aouani H, Rahmani M, Navarro-Cía M, Maier SA. Third-harmonic upconversion enhancement from a single semiconductor nanoparticle coupled to a plasmonic antenna. Nat Nanotech 2014;9:290–4.
[78] Metzger B, Schumacher T, Hentschel M, Lippitz M, Giessen H. Third harmonic mechanism in complex plasmonic Fano structures. ACS Photon 2014;1:471–6.
[79] Chen S, Li G, Zeuner F, et al. Symmetry selective third harmonic generation from plasmonic metacrystals. Phys Rev Lett 2014;113:033901.
[80] Shcherbakov MR, Neshev DN, Hopkins B, et al. Enhanced third-harmonic generation in silicon nanoparticles driven by magnetic response. Nano Lett 2014;14:6488–92.
[81] Li G, Chen S, Pholchai N, et al. Continuous control of the nonlinearity phase for harmonic generations. Nat Mater 2015;14:607–12.
[82] Yang Y, Wang W, Boulesbaa A, et al. Nonlinear Fano-resonant dielectric metasurfaces. Nano Lett 2015;15:7388–93.
[83] Chen S, Zeuner F, Weismann M, et al. Giant nonlinear optical activity of achiral origin in planar metasurfaces with quadratic and cubic nonlinearities. Adv Mater 2016;28:2992–9.
[84] Grinblat G, Li Y, Nielsen MP, Oulton RF, Maier SA. Enhanced third harmonic generation in single germanium nanodisks excited at the anapole mode. Nano Lett 2016;16:4635–40.
[85] Smirnova DA, Khanikaev AB, Smirnov LA, Kivshar YS. Multipolar third-harmonic generation driven by optically induced magnetic resonances. ACS Photon 2016;3:1468–76.
[86] Almeida E, Bitton O, Prior Y. Nonlinear metamaterials for holography. Nat Commun 2016;7:12533.
[87] Chen S, Rahmani M, Li KF. Third harmonic generation enhanced by multipolar interference in complementary silicon metasurfaces. ACS Photon 2018; DOI: 10.1021/acsphotonics.7b01423.
[88] Renger J, Quidant R, Van Hulst N, Novotny L. Surface-enhanced nonlinear four-wave mixing. Phys Rev Lett 2010;104:046803.
[89] Chen PY, Alù A. Subwavelength imaging using phase-conjugating nonlinear nanoantenna arrays. Nano Lett 2011;11:5514–8.

[90] Palomba S, Zhang S, Park Y, Bartal G, Yin X, Zhang X. Optical negative refraction by four-wave mixing in thin metallic nanostructures. Nat Mater 2012;11:34–8.
[91] Suchowski H, O'Brien K, Wong ZJ, Salandrino A, Yin X, Zhang X. Phase mismatch-free nonlinear propagation in optical zero-index materials. Science 2013;342:1223–6.
[92] Zhang Y, Wen F, Zhen YR, Nordlander P, Halas NJ. Coherent Fano resonances in a plasmonic nanocluster enhance optical four-wave mixing. Proc Natl Acad Sci USA 2013;110:9215–9.
[93] Simkhovich B, Bartal G. Plasmon-enhanced four-wave mixing for superresolution applications. Phys Rev Lett 2014;112:056802.
[94] Almeida E, Shalem G, Prior Y. Subwavelength nonlinear phase control and anomalous phase matching in plasmonic metasurfaces. Nat Commun 2016;7:10367.
[95] Nielsen MP, Shi X, Dichtl P, Maier SA, Oulton RF. Giant nonlinear response at a plasmonic nanofocus drives efficient four-wave mixing. Science 2017;358:1179–81.
[96] Kauranen M, Zayats AV. Nonlinear plasmonics. Nat Photon 2012;6:737–48.
[97] Lapine M, Shadrivov IV, Kivshar YS. Colloquium: nonlinear metamaterials. Rev Mod Phys 2014;86:1093–123.
[98] Li G, Zhang S, Zentgraf T. Nonlinear photonic metasurfaces. Nat Rev Mater 2017;2:17010.
[99] Kivshar YS. All-dielectric meta-optics and non-linear nanophotonics. Natl Sci Rev 2018;5:144–58.
[100] Burns WK, Bloembergen N. Third-harmonic generation in absorbing media of cubic or isotropic symmetry. Phys Rev B 1971;4:3437–50.
[101] Bhagavantam S, Chandrasekhar P. Harmonic generation and selection rules in nonlinear optics. Proc Indian Acad Sci A 1972;76:13–20.
[102] Lee C, Chang R, Bloembergen N. Nonlinear electroreflectance in silicon and silver. Phys Rev Lett 1967;18:167–70.
[103] Patel CKN, Van Tran N. Phase matched nonlinear interaction between circularly polarized waves. Appl Phys Lett 1969;15:189–91.
[104] Armstrong JA, Bloembergen N, Ducuing J, Pershan PS. Interactions between light waves in a nonlinear dielectric. Phys Rev 1962;127:1918–39.
[105] Fejer MM, Magel GA, Jundt DH, Byer RL. Quasi-phase-matched second harmonic generation: tuning and tolerances. IEEE J Quantum Electron 1992;28:2631–54.
[106] Zhu SN, Zhu YY, Qin YQ, Wang HF, Ge CZ, Ming NB. Experimental realization of second harmonic generation in a Fibonacci optical superlattice of $LiTaO_3$. Phys Rev Lett 1997;78:2752–5.
[107] Gabor D. A new microscopic principle. Nature 1948;161:777–8.
[108] Schlickriede C, Waterman N, Reineke B, et al. Imaging through nonlinear metalens using second harmonic generation. Adv Mater 2018; doi: 10.1002/adma.201703843.
[109] Allen L, Beijierbergen MW, Spreeuw RJC, Woerdman JP. Orbital angular momentum of light and the transformation of Laguerre-Gaussian laser modes. Phys Rev A 1992;45:8185–9.
[110] Mari A, Vaziri A, Weihs G, Zeilinger A. Entanglement of the orbital angular momentum states of photons. Nature 2001;412:313–6.
[111] Wang XL, Cai XD, Su ZE, et al. Quantum teleportation of multiple degrees of freedom of a single photon. Nature 2015;518:516–9.
[112] Wang J, Yang JY, Fazai IM, et al. Terabit free-space data transmission employing orbital angular momentum multiplexing. Nat Photon 2012;6:488–96.
[113] Li G, Chen S, Cai Y, Zhang S, Cheah KW. Third harmonic generation of optical vortices using holography based goldfork microstructure. Adv Opt Mater 2014;2:389–93.
[114] Poynting JH. The wave motion of a revolving shaft, and a suggestion as to the angular momentum in a beam of circularly polarised light. Proc R Soc Lond A 1909;82:560–7.